Research Square

Preprints are preliminary reports that have not undergone peer review.
They should not be considered conclusive, used to inform clinical practice,
or referenced by the media as validated information.

Coordinated suppression of photosynthesis- and nitrogen-related gene expression is associated with Citrus bark cracking viroid stunting in hop

Michael Hagemann

Michael.Hagemann@hs-gm.de

Hochschule Geisenheim University

Swati Jagani

University of Hohenheim

Ute Born

University of Hohenheim

Jernej Jakše

University of Ljubljana

Research Article

Keywords: Citrus bark cracking viroid (CBCVd), Humulus lupulus, hop stunting, RNA-seq, photosynthesis suppression, NRT2.5-like nitrate transporter, host accommodation

Posted Date: October 28th, 2026

DOI: https://doi.org/10.21203/rs.3.rs-10425133/v2

License: This work is licensed under a Creative Commons Attribution 4.0 International License.
Read Full License

Additional Declarations: No competing interests reported.

Coordinated suppression of photosynthesis- and nitrogen-related gene expression is associated with Citrus bark cracking viroid stunting in hop

Authors: Michael Hagemann[1,*], Swati Jagani[2], Ute Born[2], Jernej Jakše[3]

[1] Institute of Pomology (Institut für Obstbau), Hochschule Geisenheim University, Von-Lade-Str. 1, 65366 Geisenheim, Germany

[2] Department of Production Systems of Horticultural Crops, University of Hohenheim, Stuttgart, Germany

[3] Department of Agronomy, Biotechnical Faculty, University of Ljubljana, Jamnikarjeva 101, 1000 Ljubljana, Slovenia

* Corresponding author: Michael.Hagemann@hs-gm.de

ORCID: MH 0000-0002-8443-621X; SJ 0009-0001-5247-3948; UB 0009-0002-8903-9034; JJ 0000-0002-8907-1627

Keywords: Citrus bark cracking viroid (CBCVd); Humulus lupulus; hop stunting; RNA-seq; photosynthesis suppression; NRT2.5-like nitrate transporter; host accommodation

Abstract

Background. Citrus bark cracking viroid (CBCVd, *Cocadviroid rimocitri*) causes severe stunting in hop (*Humulus lupulus* L.), but the host response has rarely been resolved across

disease stages. We asked how the hop transcriptome changes between early and late season and how this relates to the whole-plant phenotype.

Results. In a 2 × 2 factorial RNA-seq experiment (CBCVd-infected vs. CBCVd-free controls × 2 post-dormancy timepoints, sampled in spring and summer, 18 and 21 months post-inoculation, respectively), with differential expression cross-validated against a second hop genome and validated by RT-qPCR and Sanger sequencing, the response was broader in May (162 differentially expressed genes, DEGs) than in August (12 DEGs), although biomass deficit was larger at the later timepoint. Only one gene, a glycine-rich cell-wall structural protein, was significant at both timepoints; the largest and most consistent suppression was found for two high-affinity nitrate-transporter (NRT2.5-like) loci, each significant at one of the two timepoints. Viroid titre was at similar height at both timepoints. At the whole-plant level, infected plants showed a leaf-chlorophyll deficit (9 % in May, 14 to 17 % from late July) and strongly reduced biomass accumulation (3 to 16 % of the control biomass across the season), in line with the transcriptome. GSEA identified coordinated suppression of photosynthesis and chloroplast function together with nitrate assimilation as the dominant signature at both timepoints, alongside repressed cell-wall and starch/sucrose metabolism. Cytosolic ribosome and translation programmes were suppressed in May but rebounded by August (treatment × timepoint interaction at pathway level), pointing to a temporal switch even as the suppression of photosynthesis- and nitrogen-related genes persisted.

Conclusions. Our data suggest that at the two analysed timepoints CBCVd-associated stunting is accompanied by an early, coordinated transcriptional suppression of photosynthesis- and nitrogen-related genes rather than the immune-signalling-dominated response reported in other viroid studies. The growth deficit is already established at the

spring sampling and persists through the season. The two NRT2.5-like loci are among the strongest and most consistent molecular correlates (log_2FC about −4 in May and −7 in August); whether they contribute to stunting or result from it, and whether they are useful as markers, remains to be tested.

Background

Most hops (*Humulus lupulus* L.) for brewing are produced within Europe, with Germany as top producer, followed by the Czech Republic, Poland and Slovenia. The most severe hop-pathogenic viroid, citrus bark cracking viroid (CBCVd), was first detected in heavily stunted hop plants in Slovenia in 2007 and later in Germany in 2019 [1, 2]. CBCVd occurs globally in citrus, where it is mostly unproblematic for commercial production, whereas in hop it causes severe stunting, bark cracking and die-back [1]. Therefore, CBCVd has prompted eradication measures in Slovenia and strict containment in Germany, making it the key viroid threat to European hop production. Its subsequent detection in Brazilian commercial hop yards in 2023 [3] further indicates that CBCVd as a hop pathogen is not restricted to Europe, extending its relevance to geographically distinct hop-producing regions. This wider occurrence adds to the need to understand CBCVd pathogenic mechanisms as a basis for future resistance strategies and disease-management approaches.

Viroids are the smallest known infectious agents of plants and can severely impact hop cultivation, with symptoms ranging from mild to devastating. Hop latent viroid (HLVd, *Cocadviroid latenshumuli*) is globally distributed and typically asymptomatic, making it the most widespread viroid in hops [4, 5]; even this symptomless viroid measurably alters hop gene expression and secondary-metabolite content, down-regulating bitter-acid and

xanthohumol biosynthesis genes in the cones [6]. Hop plants can also be infected by citrus exocortis viroid (CEVd, *Pospiviroid exocortiscitri*) through CEVd-infected citrus peels [7]; apple fruit crinkle viroid (AFCVd), endemic to Japan, induces stunting in hop [8]; and hop stunt viroid (HSVd, *Hostuviroid impedihumuli*) causes cultivar-dependent stunting [9] and has recently been confirmed for the first time in commercial hop fields in Germany [5]. Among these, *Cocadviroid rimocitri* (CBCVd) is by far the most damaging [1].

Molecular resources now support transcriptomic work in this non-model crop: a reference transcriptome of the bitter-acid and terpenophenolic pathways [10] and a hop transcriptome assembled specifically to support host-viroid research [11] provide the annotated gene space on which differential-expression analysis depends. Building on these resources, two studies have so far characterised the hop transcriptome under CBCVd, both at an advanced or pooled infection stage, and together they bracket the genome-wide response to expect. Beyond immediate antiviral defence, CBCVd infection induces alterations in core metabolic capacities. Plant nutritional status strongly shapes the ability to defend against pathogens [12], and high-affinity nitrate uptake is essential for both amino acid biosynthesis and immune signalling. The NRT2 family of high-affinity nitrate transporters, particularly NRT2.5, are key regulators of nitrogen remobilization [13]. Štajner et al. [14], profiling young leaves 28 months after biolistic inoculation of Slovenian hop cultivar 'Celeia', reported down-regulated ethylene-responsive transcription factors together with up-regulated jasmonic-acid signalling and pathogenesis-related proteins in CBCVd + HLVd co-infection, photosynthesis comparatively unaffected, and a persistent down-regulation of cell-wall genes consistent with the stunted phenotype; co-infection reduced biomass more than single CBCVd, indicating a synergistic effect. Mishra et al. [15],

pooling RNA from 4 months (pre-dormancy) and 14 months (post-dormancy) (2209 DEGs), instead found a strong suppression of photosynthesis and energy-metabolism genes with little cell-wall down-regulation. Photosynthetic suppression during viroid infection appears to be a conserved response across diverse viroid-host interactions [16]. This suppression could result in fewer cellular building blocks available for growth, potentially explaining stunting; alternatively, it may represent a host strategy to conserve energy for immune responses. Whether this represents direct damage or protective adaptation requires temporal transcriptomic resolution distinguishing early-season from late-season stages of an established infection. In faster growing, annual hosts the number of differentially expressed genes rises over the course of infection (HSVd in cucumber [17]; PSTVd [18]), so a single late or pooled hop snapshot likely captures accumulated secondary effects that mask the early, primary response.

Beyond mRNA, CBCVd also reprograms the hop small-RNA population: Mishra et al. [19] found 73 CBCVd-responsive miRNAs (36 conserved and 37 novel) in naturally infected, symptomatic (late-stage) plants, including the gibberellic-acid- and salicylic-acid-associated miR159, miR164 and miR171 families, providing a route from persistent viroid replication to sustained host reprogramming and again pointing to stage-dependent regulation.

A key unresolved question is what a contracted transcriptome signifies when viroid titre remains high: an accommodation-like host adjustment to persistent infection, or continuing metabolic damage that is no longer visible as differential expression, a distinction left unresolved by late-stage or pooled studies. Distinguishing these possibilities requires temporal transcriptomic resolution across seasonal stages of an established infection, an

approach absent from previous single-timepoint or pooled hop transcriptome analyses [14, 15].

What is still missing is a stage-resolved view of this perennial crop compared to the annually grown vegetables tested so far. Hence one aim of this study was to separate the early-season from the late-season hop response to CBCVd in an established infection and link it to the developing whole-plant phenotype. Here we resolve the hop transcriptome at two post-dormancy timepoints, in early season in spring (May) and late season before harvest (August), and integrate it with viroid titre, leaf chlorophyll content and biomass. Specifically, we asked (i) which host genes and pathways respond to CBCVd in spring and in late summer, (ii) which responses persist at both timepoints, and (iii) how these responses relate to viroid titre, leaf chlorophyll and biomass. We find that CBCVd-associated stunting is accompanied less by an active defence signature than by an early, coordinated transcriptional suppression of growth-related functions, with photosynthesis and high-affinity nitrate transport at its centre, already evident in spring and persisting as the transcriptional response narrows.

Methods

Plant material and experimental design

Eighty plants of the cultivar 'Herkules', the most widely grown variety in Germany with its typical common latent HLVd-infection, were purchased from a commercial nursery as plantlets in spring 2021 and grown in 50 L pots with standard plant protection against aphids and spider mites and sulfur against powdery mildew. The substrate was a clay-

based potting substrate (pH 5.5, starter fertilisation 1.0 g l^{-1}, extra trace elements) mixed with loamy soil (2:1). Plants were fertilised with a granular fertiliser according to plant demand following good horticultural practice and drip-irrigation. Plants grew under natural daylight without supplementary lighting. Latent viroid and virus infections are highly prevalent in commercial hop production [5]; accordingly, HLVd was detected by duplex RT-qPCR (CBCVd and HLVd probes; HLVd primers and probe after Guček et al. [20]) in all 12 pools of two plants tested in September 2022 (eight CBCVd-infected and four control pools; HLVd Ct 19 to 35), whereas CBCVd was detected only in the infected pools (Additional file 2: Table ST18). Plants were split between two greenhouse chambers slightly differing in mid-day (12:00–14:00) summer temperature and humidity: Chamber 1 averaged 27 °C and 50 % RH and Chamber 2 averaged 29 °C and 42 % RH (40 plants each, 20 per treatment). Bines were topped at about 200 cm to fit the available chamber height. No visible infected-vs-control differences appeared in 2022; biomass was therefore recorded systematically only in 2023, when all 80 plants were measured on 15 dates.

CBCVd inoculation

Two inocula were combined for a stable infection: total RNA from naturally CBCVd-infected hop, and a T7-transcribed dimeric CBCVd construct based on the full-length CBCVd variant KM211546, the variant originally described from Slovenia, to which 41 % of the CBCVd sequences from the German Hallertau outbreak were identical [21]. Each of 40 plants per treatment received 20 µg of the combined inoculum, i.e. total RNA from CBCVd-infected hop together with the dimeric CBCVd transcript (2 µg $µl^{-1}$, 10 µl), by stem injection on 18 August and 5 October 2021; controls received tap water only, without carrier RNA. The plants carried the usual latent infections of hop: HLVd and, as confirmed by our RNA-seq,

American hop latent virus (AHpLV) and hop latent virus (HpLV). The CBCVd population of the infected plants was dominated by the inoculated variant KM211546, as confirmed by sequencing of the plant material. In the RNA-seq data (the first 10 M read pairs per library that did not map to the hop reference, aligned with minimap2 to the reference genomes of AHpLV, HpLV, HLVd, HSVd and CBCVd; MAPQ ≥ 20), all 16 libraries contained AHpLV, HpLV and HLVd reads, none contained HSVd, and CBCVd reads were found in all eight infected libraries (596 to 2202 reads) but at most 7 reads in the controls, a background level consistent with index cross-talk (Additional file 2: Table ST17). Because the libraries were poly(A)-selected, these counts document presence but do not quantify viroid titre. Plants were sampled in September 2022, dormancy-treated from November 2022 (aboveground foliage removed, pots overwintered under natural conditions), and returned to the greenhouse in April 2023.

Physiological measurements

Leaf chlorophyll was measured non-destructively with an Apogee MC-100 chlorophyll concentration meter (µmol chlorophyll m^{-2}; 9 mm aperture) on five dates, and free leaf proline (per g fresh weight) on four dates across the 2023 season (assay and results in Additional file 1: Supplementary Note 1); plants overwintered as pruned rootstocks, so all plants started from zero in spring; whenever bines grew beyond the 2 m training height, the foliage above it was cut and weighed (fresh weight), these values were accumulated per plant over the season, and the whole aboveground plant was harvested and weighed at the end of the season (14 September 2023). At final harvest, root systems were inspected qualitatively by a single, unblinded observer and noted in the symptom log. Leaf chlorophyll, proline and cumulative biomass were analysed with linear mixed models

(treatment × date, chamber as fixed effect, plant as random effect; lme4 and lmerTest in R), and treatment contrasts per date are given with 95 % confidence intervals (emmeans). Chlorophyll was measured on 69 of the 80 plants (322 measurements).

RNA sequencing

Fully expanded, non-senescent, healthy leaves representative of the respective developmental stage were sampled in late May and early August 2023, i.e. at two timepoints chosen to contrast developmental stages: early season (May, ~18 months post-inoculation; vegetative elongation, BBCH 3) and late season (August, ~21 months; the phenological window of flowering/cone development, BBCH 6–7, although few cones were produced under greenhouse conditions). The design was 2 × 2 factorial (CBCVd vs. control × timepoint), four biological replicates per group, 16 libraries. Each biological replicate was a pool of leaf material from two plants; the same eight pools (four CBCVd-infected, four control; four pools per chamber) were sampled at both timepoints. On each date, leaves were collected within a single late-morning window (10:00 to 12:00) in randomised order and snap-frozen in liquid nitrogen. Total RNA was prepared with the Illumina TruSeq mRNA kit and sequenced 150 bp paired-end (27 to 73 M raw read pairs per library, median 40 M); per-library sequencing and mapping quality control is given in Additional file 1: Supplementary Note 2 and Fig. S12 and in Additional file 2: Table ST2. After trimming, 18 to 64 % of read pairs (median 27 %) mapped uniquely to the Cascade reference and 1.1 to 32.7 M fragments per library (median 5.9 M) were assigned to genes; the shallowest library, K-P1-5, was an outlier in the PCA and in the sample correlations (Fig. S12). Raw reads are available at ENA under BioProject accession number PRJEB110290.

Read processing, alignment and differential expression

Reads were adapter-trimmed with cutadapt v5.2 (TruSeq3 adapters; first 10 bases of R1 and R2 removed; reads < 50 bp discarded [22]). Trimmed reads were aligned in two-pass mode with STAR v2.7.8a [23] to the *Humulus lupulus* cv. Cascade primary assembly [24], and BAMs were sorted with samtools v1.12 [25]. Fragments per gene were counted with featureCounts v2.1.1 [26] on the gene feature (paired-end fragments, unstranded, minimum mapping quality 10). Differential expression used edgeR v4.8.2 [27]: low-count genes were removed (`filterByExpr`), libraries TMM-normalised, and quasi-likelihood GLMs were fit. CBCVd-infected and control pools were compared separately at each `timepoint` (four pools per group; a comparison between pools, therefore without a blocking factor; design ~ treatment). The treatment × timepoint interaction was tested within pools, with pool as a fixed effect (design ~ 0 + pool + August + CBCVd:August). Genes with FDR < 0.05 and $|\log_2 FC| \geq 1$ were called differentially expressed (DEGs). Sensitivity analyses with alternative models are summarised in Additional file 1: Supplementary Note 3.

Functional annotation and gene-set enrichment

DEG protein sequences (gffread v0.12.7 [28]), and a Herkules consensus generated by calling variants from the pooled BAMs with bcftools v1.22 [25], were searched against UniProt SwissProt with DIAMOND v2 ([29]; `blastp`, e-value 1e-5); about 87 % of DEGs received a hit (151 of 173; DEGs without a hit did not differ from annotated DEGs in $|\log_2 FC|$, expression level or timepoint specificity, all $P > 0.15$). GO enrichment used topGO v2.46 ([30]; elim algorithm, Fisher test, BP/MF/CC; ≥ 5 annotated genes per node) against the expressed gene set, and KEGG enrichment used *Arabidopsis thaliana* as a proxy mapping

(best SwissProt hit, then the UniProt-to-KEGG Arabidopsis gene; Fisher test, Benjamini-Hochberg). This mapped 3173 of 18,130 tested genes (17 %) and 25 of 162 May DEGs (15 %) to a KEGG pathway, and 73 % of the mapped hop genes shared their Arabidopsis gene with another hop gene, so KEGG results are interpreted with caution and complemented by GO (140 of 162 May DEGs and 10 of 12 August DEGs carried GO annotation). To capture coordinated sub-threshold shifts, gene-set enrichment analysis (GSEA; [31]) was run with fgsea v1.36.2 [32] on the full ranked list (rank = sign($\log_2$FC) × −$\log_{10}$P) per timepoint and for the treatment × timepoint interaction (minSize 5, maxSize 500, eps 0, seed 42), reporting normalised enrichment scores (NES) and Benjamini-Hochberg-adjusted p-values (Additional file 1: Supplementary Note 4); the full GO and KEGG enrichment results are given in Additional file 2: Table ST7. The 22 DEGs without a SwissProt hit were additionally searched with blastn against NCBI core_nt restricted to Viridiplantae (E < 1e-5); 19 of them matched a *Humulus lupulus* transcript and are named accordingly in Additional file 2: Tables ST3 to ST5, with the full hit list in Table ST20.

qPCR and Sanger validation

CBCVd infection and viroid titre (Fig. 1A) were determined on the same eight pools used for RNA-seq (repeated measurements gave consistent results) by reverse-transcription duplex real-time PCR on total RNA extracted with the Monarch Total RNA Miniprep Kit (New England Biolabs), using a FAM-labelled CBCVd probe with the plant mitochondrial nad5 (NAD) gene as internal control and 0.2 µl and 1 µl template volumes, following the validated protocol of Jagani et al. [33]. Several candidate DEGs, chosen among the strongest and most consistent DEGs of the initial analysis before the statistical model and the read counting were revised, were assayed by RT-qPCR with gene-specific primers (Primer3 v2.3.0 [34];

designed on the Herkules consensus CDS), of which seven yielded efficient, usable assays and were used for validation (the TP1A primers also match two paralogous loci); RNA extraction, cDNA synthesis and qPCR followed Hagemann et al. [35], using the hop 7SL reference gene validated therein against four candidates by BestKeeper, with per-amplicon efficiencies determined from the raw fluorescence curves and a pooled-cDNA "Linker" sample as inter-run calibrator. The qPCR amplicons of the significant differentially expressed genes were checked for identity by Sanger sequencing at Macrogen Europe (Amsterdam, The Netherlands); reads were quality trimmed in Biopython v1.86 [36], assembled into per-amplicon consensus sequences and identified by BLASTn against the target transcripts (Additional file 1: Supplementary Note 5; consensus sequences in Table ST11).

Reference cross-validation

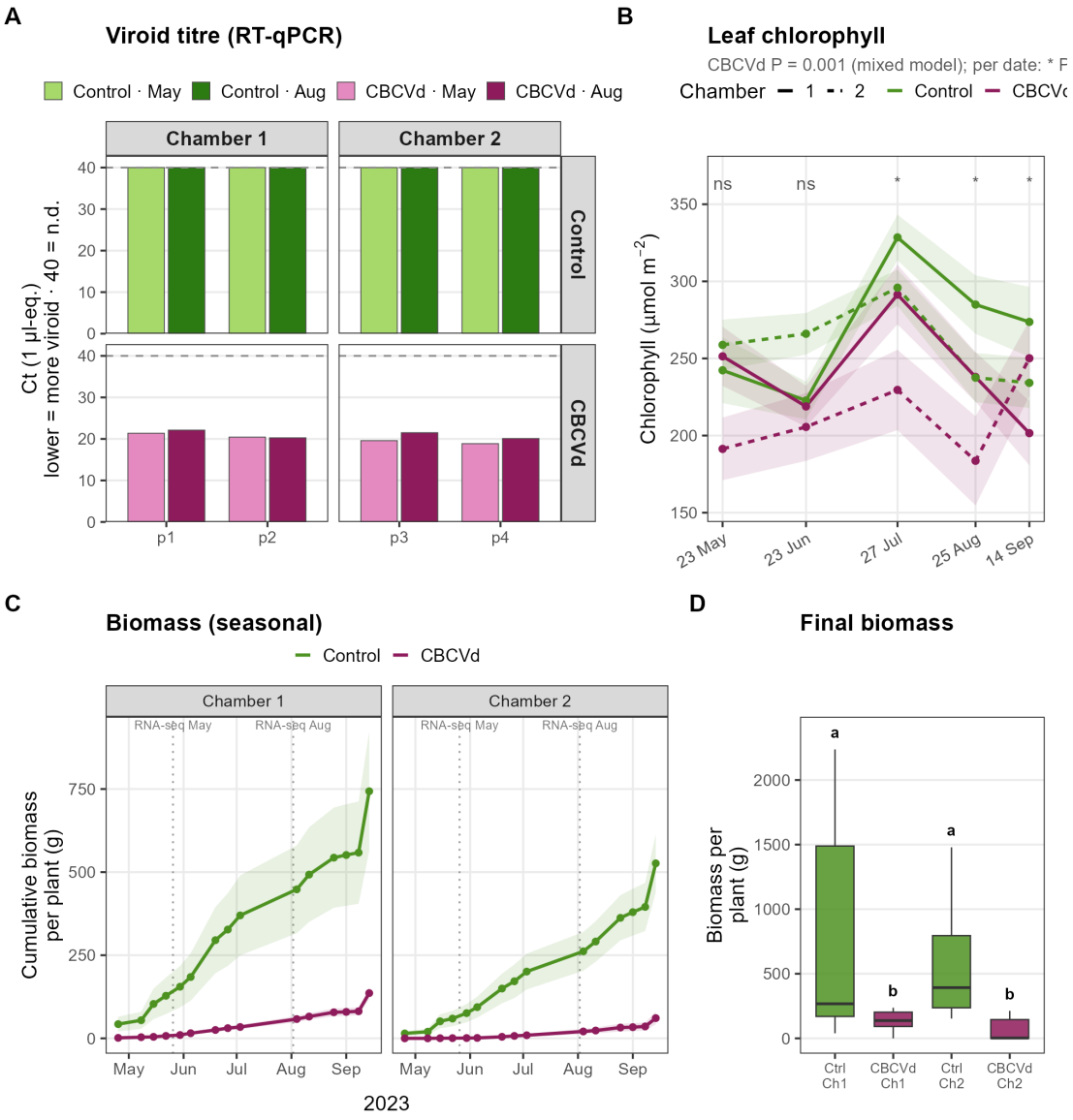
A three-reference mapping benchmark against "Cascade" [24], the European chromosome-level "Kew" genome drHumLupu1.1 (GCA_963169125.1) and the "Apollo" assembly (GCA_963992765 [37]) confirmed Cascade as the best available reference; Apollo gave no gain in uniquely mapped reads and, as a very recent assembly, lacks a public annotation matching its released haploid genome, so the differential-expression cross-validation used Cascade and Kew (Additional file 1: Supplementary Note 6). DEGs were also called against the Kew genome with the same counting and model; of the Cascade DEGs with a reciprocal-best-hit ortholog tested in Kew (98 of 162 in May, 8 of 12 in August), all agreed in direction, and $\log_2$FC values correlated closely ($r = 0.99$ at both timepoints; $r = 0.95$ in May and 0.92 in August across all 11,232 and 10,087 orthologous pairs tested) (Additional file 2: Tables ST12 and ST13). The three references yielded the same share of uniquely mapped reads on

average (Cascade 30.4 %, Kew 31.2 %, Apollo 30.7 %). The hop NRT2 family was assembled from best SwissProt hits (five genes), aligned with MAFFT, and a FastTree (LG model) tree was rooted on Arabidopsis NPF6.3 (Additional file 1: Supplementary Fig. S13; Additional file 2: Table ST14).

Results

CBCVd infection, titre and the stunting phenotype

RT-qPCR confirmed CBCVd in all infected plants and its absence in the CBCVd-negative controls (Fig. 1A; the reference gene NAD was detected at the same level in all samples). Viroid titre was high at the same level at both timepoints (mean CBCVd Ct, normalised to a 1 µl template equivalent by combining the 1 µl and 0.2 µl reactions as described for Fig. 1A: 19.9 in May and 21.1 in August), so the infection is already well established at the early-season sampling. Leaf chlorophyll was lower in infected plants across the season (Fig. 1B), and infected plants accumulated strongly reduced biomass in both chambers while controls grew on (Fig. 1C,D; treatment × date interaction $P < 0.001$ in the mixed model; final-harvest difference −607 g in Chamber 1 and −466 g in Chamber 2). Infected plants were smaller than controls at the first measurement in April and at the last biomass measurement before the May sampling (22 May: 4.0 g vs. 93.8 g cumulative fresh weight per plant, about 4 % of the controls); their biomass was 11 % of the control biomass on 4 August and 16 % at final harvest. The absolute whole-plant deficit therefore widens across the season, whereas titre is already high early.



286

287 **Fig. 1. CBCVd infection is associated with lower leaf chlorophyll and reduced biomass**

288 **accumulation. (A)** Viroid titre as relative viroid load (model-based 1 µl-equivalent Ct,

289 amplification efficiency E ≈ 98 %), per pool and split by climate chamber; CBCVd is detected

290 in all infected pools at both timepoints and absent from controls (load ≈ 0, Ct = 40); titre

291 does not differ between May and August (t-test p = 0.25, n = 4 pools). **(B)** Leaf chlorophyll

292 (Apogee MC-100, µmol m^{-2}) across the 2023 season, consistently lower in infected plants;

293 line type = climate chamber; per-date CBCVd contrasts from the linear mixed model

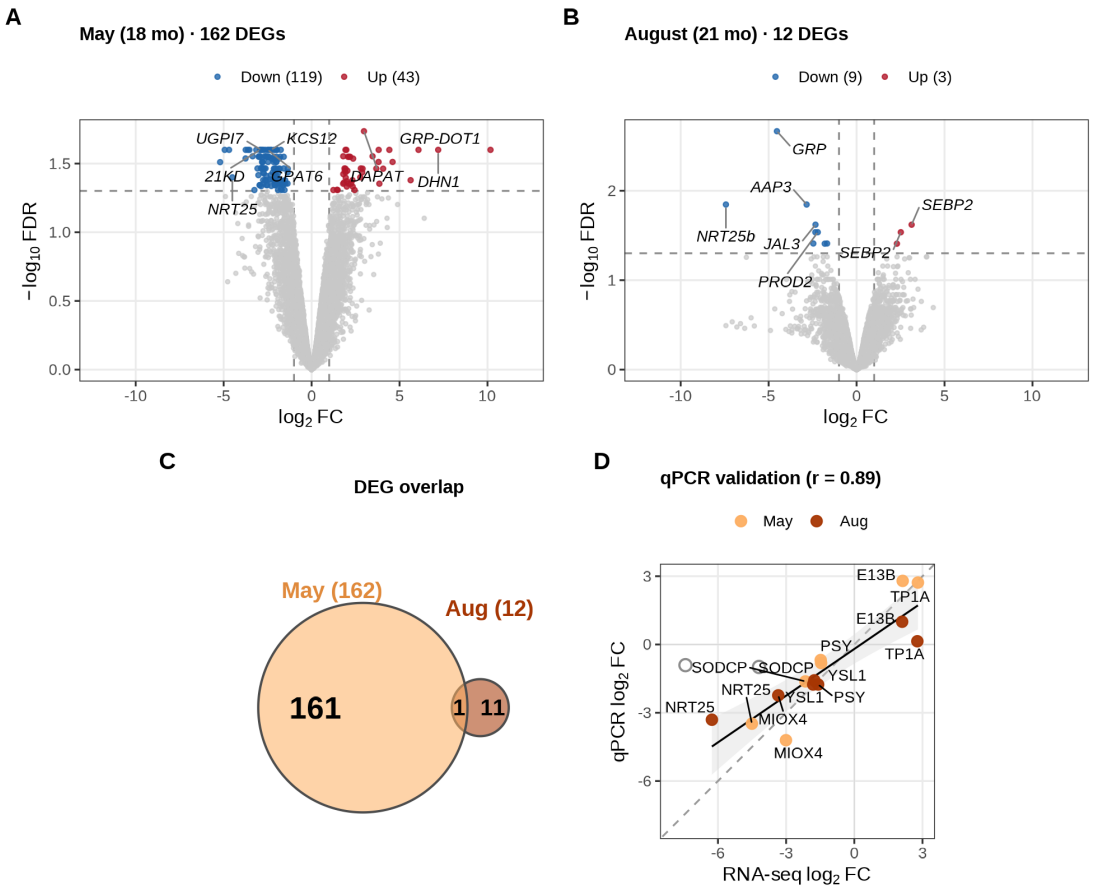
annotated (* P < 0.05, ns = not significant), CBCVd effect P = 0.001. **(C)** Cumulative biomass per plant (mean ± SE), one panel per climate chamber; dotted lines mark the RNA-seq sampling dates (26 May and 2 August 2023). **(D)** Final-harvest biomass by treatment × chamber (n = 20 per group); letters = Tukey HSD groups (p < 0.05). Green = CBCVd-negative control, magenta = CBCVd-infected.

The transcriptional response is broader in May than in August

A 2 × 2 factorial RNA-seq experiment (16 libraries) against the *H. lupulus* cv. Cascade reference gave markedly different DEG numbers at the two timepoints (Table 1): 162 DEGs in May but only 12 in August. The broader response is in May, when infected plants are already much smaller than controls in relative terms, whereas August shows a narrower response although the absolute biomass deficit is larger and titre is comparable. Effect sizes were similar at both timepoints (median $|\log_2 FC| \approx 2.3$); the difference lies in the number of genes regulated, not their magnitude. The treatment × timepoint interaction, tested within pools, was significant for only 12 genes (Additional file 2: Table ST6), so the May-vs-August difference in DEG number mainly describes response breadth at the chosen threshold and should not be read as a statistically demonstrated change of the CBCVd effect for most genes; at the pathway level the interaction is significant (see below). Only 1 DEG is shared (161 May-specific, 11 August-specific; Fig. 2C), which describes the overlap of two thresholded gene lists. Nine genes differed significantly in the CBCVd effect between the timepoints; among them are two small heat-shock protein genes (HS21C) that were up-regulated in May and strongly down-regulated in August.

Table 1. DEGs per contrast (Cascade, FDR < 0.05 and $|\log_2 FC| \geq 1$).

Contrast	DEGs	Down	Up
May (18 mo post-inoculation)	**162**	119	43
August (21 mo)	**12**	9	3
Persistent (May ∩ August)	**1**	1	0



316

317 **Fig. 2. The CBCVd-responsive transcriptome. (A, B)** Volcano plots, CBCVd vs control
318 (Cascade), May (A) and August (B); blue = significantly down, red = up (FDR < 0.05 and
319 $|\log_2 FC| \geq 1$), grey = ns; labels = gene symbols of the strongest hits and of the NRT2.5-like
320 loci and DHN1 where they pass the threshold. May 162 DEGs (119↓/43↑), August 12 DEGs
321 (9↓/3↑). **(C)** Overlap of May and August DEGs (161 May-specific, 11 August-specific, 1
322 shared). **(D)** qPCR validation: RNA-seq vs qPCR $\log_2 FC$ (orange = May, dark red = August);

line = regression (± 95 % CI), dashed = 1:1; NRT25b (NRT2.5-like locus 2, 006054F.g2) excluded from the fit (primer efficiency 72 %, grey open circles); overall r = 0.89.

Functional enrichment: coordinated suppression of photosynthesis- and nitrogen-related gene sets

In May the over-representation signal is dominated by the cell wall and apoplast (cellulase activity, cellulose catabolic process, pectinesterase inhibitor activity, plant-type cell wall; extracellular region, 50 of 723 annotated genes), together with peroxidase and hydrogen-peroxide catabolism and systemic acquired resistance; by KEGG, metabolic pathways (27 of 1336) and starch and sucrose metabolism (6 of 107) are enriched. In August only small gene sets are enriched, each with two or three DEGs, led by nitrate transmembrane transport and nitrate assimilation (2 of 11 and 2 of 25 annotated genes) and, by KEGG, nitrogen metabolism (2 of 15); the full per-timepoint over-representation results (GO P values are topGO elim values and not adjusted) are in Additional file 2: Table ST8.

This apparent loss of the plastid signal reflects the small August DEG count rather than recovery: as shown in Fig. 3 GSEA on the full ranked lists shows photosynthesis and chloroplast suppression at both timepoints (chloroplast thylakoid membrane NES −2.88 in May, padj 3×10^{-43}, and −2.61 in August, padj 2×10^{-24}; photosystems I/II; reductive pentose-phosphate cycle; Additional file 2: Table ST7), together with suppressed nitrogen transport and assimilation (ammonium transmembrane transport NES −1.81, padj 0.02 in May; nitrate transmembrane transport NES −2.07, padj 0.005, and nitrate assimilation NES −1.96, padj 0.01, in August). Cytosolic ribosome and translation show a temporal switch: significantly suppressed in May (structural constituent of ribosome NES −2.19) but

activated by August (NES +2.17; KEGG Ribosome −2.26 in May and +1.78 in August), while organellar translation stays suppressed. The switch is supported by a significant treatment × timepoint interaction at the pathway level (structural constituent of ribosome NES +2.91, padj 8×10^{-28}; translation NES +2.60; plant-type cell wall NES +2.12; response to heat NES −1.86; Additional file 2: Table ST7). GSEA therefore places photosynthesis/chloroplast-related and nitrogen-related gene sets, not ribosome biogenesis, at the persistent coordinated-suppression core (Fig. 3; full GO/KEGG maps and ridges in Additional file 1: Supplementary Fig. S5–S8).

Beyond the nitrogen-centred signature, the KEGG ridge plots (Fig. 3) show that several metabolic classes shift over the season rather than staying uniformly repressed. Central carbon fixation and energy metabolism (Calvin-cycle carbon fixation, photosynthesis antenna proteins, ubiquinone/terpenoid-quinone metabolism) are suppressed at both timepoints (KEGG NES −1.8 to −2.0 for Calvin-cycle carbon fixation and photosynthesis in May; weaker and not significant at the KEGG level in August). Fatty-acid and central-carbon metabolism reconfigure over time: β-oxidation and citrate-cycle activity are repressed in May, whereas August shows up-regulation of fatty-acid degradation, proteasome and ubiquitin-mediated proteolysis. Amino-acid metabolism switches similarly, with arginine/proline and glycine/serine/threonine pathways suppressed in May but trending towards activation by August. These time-dependent shifts are interpreted in the Discussion.

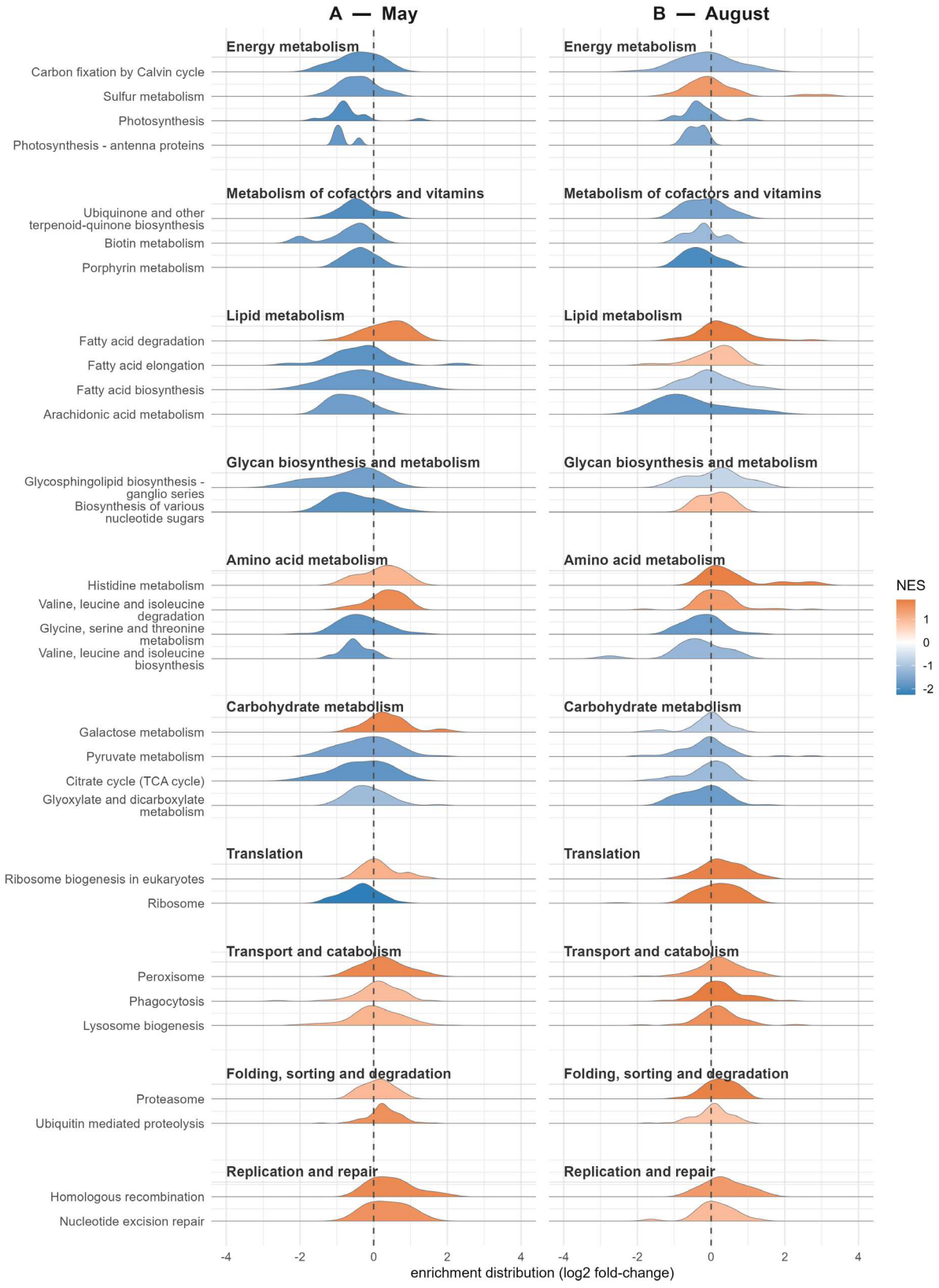

A — May
B — August
Energy metabolism
Carbon fixation by Calvin cycle
Sulfur metabolism
Photosynthesis
Photosynthesis - antenna proteins
Metabolism of cofactors and vitamins
Ubiquinone and other terpenoid-quinone biosynthesis
Biotin metabolism
Porphyrin metabolism
Lipid metabolism
Fatty acid degradation
Fatty acid elongation
Fatty acid biosynthesis
Arachidonic acid metabolism
Glycan biosynthesis and metabolism
Glycosphingolipid biosynthesis - ganglio series
Biosynthesis of various nucleotide sugars
Amino acid metabolism
Histidine metabolism
Valine, leucine and isoleucine degradation
Glycine, serine and threonine metabolism
Valine, leucine and isoleucine biosynthesis
Carbohydrate metabolism
Galactose metabolism
Pyruvate metabolism
Citrate cycle (TCA cycle)
Glyoxylate and dicarboxylate metabolism
Translation
Ribosome biogenesis in eukaryotes
Ribosome
Transport and catabolism
Peroxisome
Phagocytosis
Lysosome biogenesis
Folding, sorting and degradation
Proteasome
Ubiquitin mediated proteolysis
Replication and repair
Homologous recombination
Nucleotide excision repair
NES
1
0
-1
-2
-4
-2
0
2
4
enrichment distribution (log2 fold-change)

Fig. 3. Coordinated metabolic reprogramming (GSEA, fgsea), May (A) vs August (B). KEGG gene sets grouped by functional class; each ridge = density of member-gene $\log_2$FC, colour = NES (blue = suppressed, red = activated), dashed line = 0; the x-axis is fixed to [−4, 4] $\log_2$ fold-change. Energy metabolism (Calvin cycle, photosynthesis) is suppressed at both timepoints, while the Translation block flips from suppressed (May) to activated (August).

A persistent core led by a nitrate transporter

Only one gene is significant at both timepoints: the glycine-rich cell-wall structural protein GRP (006438F.g4), repressed by $\log_2$FC −3.62 (FDR 0.025) in May and −4.53 (FDR 0.0022) in August. The down-regulated set is led by a high-affinity nitrate-transporter (NRT2.5-like, "NRT25") locus (000404F.g19) whose suppression deepens from $\log_2$FC −4.5 in May to −6.3 in August, alongside GRP, SODCP (chloroplastic Cu/Zn superoxide dismutase), PSY (phytoene synthase) and three genes on the same scaffold without SwissProt hit (002581F.g2, g5 and g12); the only up-regulated gene is the pathogenesis-related protein E13B. The second NRT2.5-like locus (006054F.g2) has a similar effect size ($\log_2$FC −4.2 in May, −7.4 in August) and passes the significance threshold only in August, whereas the first passes it only in May (FDR 0.040 in May, 0.055 in August), and the dehydrin DHN1 ($\log_2$FC +7.2 in May) only in May. Together, the two NRT25 loci show the largest and most consistent effects across the season, with progressively stronger repression.

The annotation of GRP rests on nucleotide BLAST: 006438F.g4 returned no SwissProt blastp hit (glycine-rich, low-complexity composition, which is masked by default protein-search filters); it was assigned by nucleotide BLAST (blastn) with 100 % identity to Humulus lupulus glycine-rich cell wall structural protein-like (LOC133795330;

XM_062232783.1) and to the drHumLupu1.1 chromosome 8, and 92–99 % to the Apollo assembly [37].

qPCR-Validation of differential expression

We tested several candidate DEGs by qPCR (7SL reference, ΔΔCt with a linker calibrator); seven yielded usable assays and were used for validation (NRT25b, 006054F.g2, was excluded for low primer efficiency, 71.9 ± 6.9 %; melt-curve analysis of this assay showed a primer-dimer at a melting temperature of about 71 °C alongside the specific product at about 82 °C, whereas the NRT25 assay, which shares the forward primer, gave a single product at about 81 °C, so competition by the dimer is the most likely cause of the reduced efficiency). Across these seven genes qPCR and RNA-seq $\log_2$ fold changes agreed in direction at both timepoints and were strongly correlated (overall Pearson r = 0.89, R^2 = 0.80; May r = 0.96; August r = 0.96; Fig. 2D), and the qPCR amplicons of the significant genes were checked for identity by Sanger sequencing (Additional file 1: Supplementary Note 5). A leave-one-out analysis across libraries showed that the effect sizes of the core genes were stable, whereas the number of genes passing the significance threshold varied; GRP remained significant in five of eight May runs and in all eight August runs (Additional file 2: Table ST16).

Discussion

Phenotype and transcriptome are consistent with reduced growth

At the whole-plant level, CBCVd infection is associated with a growth deficit that widens in absolute terms across the season, although the pathogen is well established and the

infected plants are markedly smaller as early as May (Fig. 1A,C). Leaf chlorophyll is lower in infected plants (Fig. 1B) and biomass accumulation is strongly reduced in both climate chambers (Fig. 1C,D), while viroid titre is on an overall high level with no difference between the two time points assessed (Fig. 1A). This whole-plant deficit is in line with the severe biomass penalty reported for CBCVd in hop by Štajner et al. [14], who measured a 54 % biomass reduction under single CBCVd infection and 81 % under CBCVd and HLVd co-infection, which is consistent with the stunting we quantify here.

The transcriptome points to the same lesion from the molecular side: the strongest enrichment signal is a coordinated suppression of photosynthesis and chloroplast function (Fig. 3), together with downregulation of nitrate assimilation. That two independent lines of evidence, a whole-leaf chlorophyll deficit and a genome-wide suppression of photosynthesis-related transcripts, point to the same process is a central result of this study. Our findings are consistent with an early loss of growth capacity, followed by adaptation of the plant at a stunted level; because the study is observational, we cannot distinguish whether the transcriptional changes cause the stunting, result from it, or arise in parallel. In the following we discuss how this fits into the recent body of viroid knowledge.

Two seasonal stages of the response

Following the hop response to CBCVd across two post-dormancy timepoints revealed a temporal decoupling between the breadth of the transcriptional response and the severity of disease. In May (18 months post-inoculation) the response is broad, with 162 DEGs spanning cell-wall biosynthesis, plastid function, nitrate assimilation and a pronounced

ABA-associated drought-like programme, reflected by the ABA/water-deficit-induced transcription factor *ATHB7* [38] and the dehydrin *DHN1* [39], alongside the ABA-modulator *MFT*. At this stage the infected plants are already markedly smaller than the controls (Fig. 1C). Extensive transcriptome changes have also been detected early in other viroid infections, for example in HSVd-infected cucumber at 10 dpi, when systemic viroid RNA is present but macroscopic symptoms are not yet evident [17]; in our system, however, the May sampling took place 18 months after inoculation, in plants that were already stunted. Free leaf proline, a marker of osmotic stress, was strongly elevated in infected plants on the May sampling date, but not at later dates, nor in August 2022, when no symptoms were visible (Additional file 1: Supplementary Note 1), which fits the ABA- and dehydrin-associated signature in May. By August (21 months) the transcriptional response narrows to 12 DEGs and the ABA-associated programme is less prominent, even though the absolute biomass deficit is larger while viroid titre remains high (Fig. 1). One possible interpretation is a broader transcriptional response in spring followed by a smaller, sustained core of changes in late season that is associated with persistent growth failure. The treatment × timepoint interaction supports this at the pathway level (cytosolic ribosome and translation, cell wall, heat response) but was significant for only 12 individual genes, and May and August also differ in developmental stage (BBCH 3 vs. 6–7) and leaf age; this two-stage description is therefore an interpretation of the data and not a statistically demonstrated transition. This stunting corresponds to the typical described endpoint of the CBCVd infection in hops [1].

Growth-suppression instead of defence-domination

The strong jasmonic acid, ethylene and pathogenesis-related protein activation that dominates the late-stage and pooled studies [14, 15] is not seen in this study, since we detect only a modest response of the pathogenesis-related proteins TP1A and E13B. Štajner et al. [14], sampling at 28 months, reported induced jasmonic acid signalling and pathogenesis-related proteins together with down-regulated ethylene-response factors, and Mishra et al. [15] likewise found jasmonate and ethylene induction alongside a strong suppression of photosynthesis and energy metabolism. Interpreted against the literature, this is compatible with active defence signalling being a comparatively late reaction to accumulated damage, whereas the earliest event detectable in our data is a coordinated suppression of anabolic capacity: photosynthesis and chloroplast function, nitrate assimilation, starch/sucrose and ascorbate metabolism, and cell-wall synthesis. The cell-wall arm of this suppression is notable given the eponymous bark-cracking symptom of CBCVd: two expansins (EXP10, EXPB3) are strongly down-regulated in the acute May phase, and a glycine-rich cell-wall structural protein (006438F.g4, identified here by nucleotide BLAST) is among the persistently repressed core genes, whereas the only induced cell-wall enzyme is the pathogenesis-related β-1,3-glucanase E13B; a sustained loss of structural cell-wall proteins is consistent with the mechanical weakening that manifests as stem bark cracking, but bark-cracking severity was not quantitatively related to the expression of these genes. Taken together, the opposite regulation of the most persistent genes, with repression of the glycine-rich cell-wall structural protein GRP and induction of the dehydrin DHN1 and the thaumatin-like pathogenesis-related protein TP1A, is consistent with a shift from growth and cell-wall build-up towards ABA-dependent

protective proteins and a weak basal defence. Based on our findings, the transcriptional signature may be better described as a suppression of growth-related functions than as an immune-signalling-dominated response, which is involved in some phases of the CBCVd-pathology [14, 15], but those studies did not analyse the early-season and very late stages.

NRT2.5-like genes as a candidate molecular correlate

The most consistent and progressively worsening signal of the dataset is the suppression of two high-affinity nitrate-transporter (NRT2.5-like) loci, deepening from $\log_2$FC about −4 in May to about −7 in August; the first locus is significant in May and was confirmed by qPCR, whereas the second (NRT25b) is significant only in August and was excluded from the quantitative qPCR validation because of low primer efficiency; for NRT25b, qPCR agreed with RNA-seq in direction at both timepoints but not in magnitude, which melt-curve analysis attributes to a primer-dimer competing with the specific amplicon (Additional file 1: Supplementary Note 5). Both loci are the closest hop homologues of Arabidopsis NRT2.5 (74 % AA ID) and cluster with it in a phylogeny of the hop NRT2 family, whereas the three other hop NRT2 genes (one scaffold) cluster with NRT2.1 to NRT2.4 (Additional file 1: Supplementary Fig. S13). In *Arabidopsis thaliana*, NRT2.5 drives high-affinity nitrate acquisition and remobilisation specifically under prolonged nitrogen starvation [13], so sustained loss of these loci in a high-nitrogen-demand perennial suggests a hypothesis linking transcriptional suppression to the stunting phenotype. Nitrate uptake, tissue nitrogen and nitrate reductase activity were not measured, so the data cannot distinguish whether NRT2.5-like repression contributes to stunting, results from the lower nitrogen demand of already stunted plants, or arises in parallel. The repression of the NRT2.5-like loci is accompanied by concurrent repression of genes for chloroplast redox homeostasis

(SODCP), carotenoid biosynthesis (PSY) and ascorbate metabolism (MIOX4), suggesting that it is part of a broader transcriptional suppression of growth-supporting metabolism. Beyond nutrition, nitrate transporters integrate nitrogen status with defence and stress signalling via nitric oxide and reactive oxygen species [40], so their sustained repression may compound the growth deficit with impaired stress signalling. Nitrogen acquisition has not been reported in previous hop-viroid transcriptomes [14, 15], and the two NRT25 loci emerge here as the molecular correlates with the largest and most consistent effect sizes of CBCVd-associated stunting in the cultivar Herkules. If this repression limits nitrogen acquisition, stresses such as pot culture or nitrogen limitation could aggravate stunting that nitrogen supplementation might rescue, consistent with differing susceptibility ratings of some cultivars in field assessments (personal communication).

A qualitative root observation at final harvest is consistent with, but does not test, this nitrogen-acquisition interpretation. A single, unblinded inspection noted that CBCVd-infected plants had a flatter and thinner root system than controls, with fine roots concentrated in the upper half of the pot and unevenly distributed, and microroots marginally thinner than in controls. Rooting volume was reduced and shallower, without necrosis. Because root traits and nitrate uptake were not quantified, this qualitative pattern cannot establish a causal link to NRT2.5-like repression. Still, a smaller root system would be expected to lower high-affinity nitrate acquisition, which depends partly on root architecture [41], so both effects could act in the same direction.

Suppression of photosynthesis-related genes and a cytosolic translational switch

Beyond the threshold-based DEG view, GSEA on the full ranked transcriptome resolves coordinated shifts below the DEG threshold (Fig. 3). The photosynthesis block is suppressed at both timepoints and remains strongly suppressed in August (chloroplast thylakoid membrane NES −2.61, versus −2.88 in May) although far fewer individual genes pass the DEG threshold then, pointing to reduced carbon-fixing capacity as a central feature, although photosynthesis was not measured directly, and matching the whole-leaf chlorophyll reduction, which is stronger late in the season (Fig. 1B). Suppression of photosynthesis and chloroplast function is a canonical viroid response across hosts [16, 17] and scales with disease severity [42], so our GSEA thylakoid signal is mechanistically consistent rather than hop-specific. Unexpectedly, cytosolic ribosome and translation programmes are not uniformly repressed: they are suppressed in May but rebound to significant activation by August (structural constituent of ribosome NES −2.19 in May, +2.17 in August), while plastid and mitochondrial translation stays down regulated. We tentatively interpret this as a possible host attempt to restore cytosolic protein synthesis once the acute transcriptomic dysregulation in May passes, even as the suppression of chloroplast- and nitrogen-related genes, which may contribute to biomass loss, persists. To our knowledge a suppression-then-recovery of cytosolic translation has not been explicitly reported for persistent viroid infection, so we present this as an observation that remains to be confirmed. This temporal switch is invisible to a contrast averaged over both timepoints and is captured by the treatment × timepoint interaction; it revises the intuitive assumption that ribosome biogenesis belongs to the persistent suppression core. Independent evidence that proteosynthesis components are viroid-responsive in hop

comes from HLVd-infected plants, where altered expression of ribosomal protein L5 (RPL5) and altered splicing of transcription factor IIIA-7ZF suggest that the RPL5/TFIIIA-7ZF regulatory cascade may also contribute to viroid replication [6].

The persistent suppression of chloroplast-centred carbon fixation, together with the late up-regulation of catabolic recycling (fatty-acid degradation, proteasome, ubiquitin-mediated proteolysis; Fig. 3), fits the general source-to-sink transition and primary-metabolic reprogramming that Llave [43] describes for plant virus infections, in which photosynthesis is transcriptionally repressed and carbon, nitrogen and lipid metabolism are reallocated to meet the combined demands of pathogen maintenance and host defence. Unlike plant viruses, CBCVd is a viroid that encodes no proteins and forms no membrane-bound replication complexes, yet infection is still associated with reduced photosynthetic carbon capture and increased turnover of lipids and proteins under chronic stress. Accordingly, the early repression of respiration-linked TCA and amino-acid metabolism and the later shift towards catabolic recycling are interpreted as a viroid-associated instance of the metabolic-acclimation pattern known from plant–virus interactions.

Stage-dependent viroid pathology

The narrower response in August is a notable, unexpected feature of our time-resolved data, and it is best judged against pathosystems in which the transcriptome has been resolved over time. In faster, annual hosts the response breadth grows with infection: HSVd in cucumber rises during early infection from 10 DEGs at 10 dpi, over 55 DEGs at 17 dpi, and 271 DEGs at 24 dpi [17]. PSTVd infected tomato roots accumulates 3469 DEGs across 17, 24 and 49 dpi, also peaking late [18], while a comparable progression has been shown

563 in potato leaves [44]. Hop runs counter to this annual rule even on a matched threshold: its
564 response falls from 162 to 12 DEGs while titre is unchanged, so the number of DEGs is
565 higher in spring than in late season; the difference in gene counts alone does not
566 demonstrate a change in the CBCVd effect, but the pathway-level interaction (ribosome and
567 translation, cell wall, heat response) indicates that the response also differs qualitatively.

568 At the pathway level, by contrast, our signal is not an outlier but part of a broader pattern.
569 Host transcriptome reprogramming around the same metabolic nodes is documented
570 across RNA and DNA viruses beyond viroids: a time-resolved, strain-severity-dependent
571 response to bean common mosaic virus in common bean [45], photosynthesis suppression
572 accompanying dwarfing under wheat dwarf virus in wheat [46], and mitochondrial
573 metabolic and redox reprogramming under bamboo mosaic virus in *Nicotiana benthamiana*
574 [47]. Photosynthesis, energy metabolism and redox balance are thus recurrent nodes of
575 viral and viroid symptom development, even where the temporal trajectory of the response
576 differs between hosts.

577 Within hop, developmental stage and infection age also reconcile our gene-level findings
578 with the two earlier datasets, which on the surface appear to conflict. Štajner et al. [14]
579 sampled a single late stage, after a second dormancy, but after 28 months post-infection
580 compared to our 21 months, and reported photosynthesis as comparatively unaffected with
581 a defence-dominated signature (JA up, PR up, ERF down). Mishra et al. [15], pooling pre-
582 dormancy (4 months) and post-dormancy (14 months) leaves (2209 DEGs), instead found
583 strong suppression of photosynthesis and energy metabolism with little cell-wall
584 downregulation. Our GSEA resolves the apparent conflict: photosynthesis/chloroplast
585 suppressed at both timepoints and strongest in August (Fig. 3; Additional file 1:

Supplementary Fig. S5–S6), an early, primary event that the late-only window of Štajner et al. [14] might have missed, while the cell-wall downregulation those authors emphasised appears in our data as an acute May feature, mirroring the early, cell-wall-dominated phase of PSTVd in tomato roots [18].

Host accommodation

One possible explanation for the narrower response in August while titre remains high is host accommodation, in which a perennial host survives persistent infection through transcriptional and metabolic remodelling rather than pathogen elimination [48, 49]. Alternative explanations include developmental differences between BBCH 3 and BBCH 6–7, leaf age, changes in source–sink relationships and cell-type composition, and a general reduction of metabolic activity in severely stunted plants. The support for this in our data is a stage-dependent shift of the hormone axis: our early window is dominated by an ABA/drought-like programme (DHN1, ATHB7, MFT) that is much less prominent among the August DEGs (DHN1 itself remains induced, $\log_2$FC +5.2), whereas Mishra et al. [19] reported gibberellic-acid- and salicylic-acid-associated miRNAs at a late symptomatic stage, a trajectory consistent with stress-then-accommodation. Beyond this, the mechanism of the contraction is not testable from our mRNA data, and the following are candidate routes only. RNA-directed silencing by reprogrammed host and viroid-derived small RNAs is plausible, since CBCVd reprograms the hop microRNA population [19] and hop viroid-derived sRNAs are predicted to target over a thousand transcripts, including hormone-metabolism and small-RNA-biogenesis genes [11]; and RNA-directed DNA methylation could entrench an accommodated state, since CBCVd-infected hop shows altered methylation consistent with an active RdDM pathway [50]. A contraction or normalisation

of the transcriptome during ongoing infection has also been reported for tobacco and tomato [51, 52]. Which of these, if any, underlies the narrower late-season response is an open question that stage-resolved small-RNA sequencing and methylome profiling on the same material could resolve.

The design is observational and compares infected with control plants within each of two timepoints that also differ in developmental stage, so the seasonal contrast is descriptive; and the physiological measurements that would test the nitrogen-acquisition reading (nitrate uptake, tissue nitrogen, gas exchange) were not part of this experiment, which had ended before the NRT2.5-like result emerged. The plant material was certified nursery stock of the leading German cultivar and carried the latent viroid and virus infections that are prevalent in commercial hop [5]; the CBCVd effects reported here were therefore measured against this background. The effect sizes of the core genes were robust to sequencing depth and library composition (Additional file 1: Supplementary Note 2; Additional file 2: Table ST16), whereas the number of genes crossing the significance threshold was not.

Conclusion

A stage-resolved transcriptome, together with whole-plant chlorophyll and biomass data, shows that CBCVd-associated stunting in hop is accompanied less by an active defence signature than by an early, coordinated transcriptional suppression of growth-related functions (photosynthesis, nitrogen-related genes and cell-wall metabolism), already present in spring in plants that are then persistently smaller than controls, while the transcriptional response narrows in late season. The two NRT25 nitrate-transporter loci

show the largest and most consistent effects among the genes associated with the phenotype in the cultivar Herkules. Whether they contribute to stunting, result from it, or are useful as markers or management targets remains to be tested, for example by direct measurements of nitrate uptake and tissue nitrogen, functional assays, and validation in independent plants and cultivars.

List of abbreviations

CBCVd, Citrus bark cracking viroid; HLVd, Hop latent viroid; DEG, differentially expressed gene; GSEA, gene-set enrichment analysis; NES, normalised enrichment score; ORA, over-representation analysis; FDR, false discovery rate; BBCH, growth-stage scale.

Declarations

Ethics approval and consent to participate

Not applicable, the study used cultivated hop (*Humulus lupulus*); no human or animal subjects.

Consent for publication

Not applicable.

Availability of data and materials

The raw sequencing reads generated in this study are available in the European Nucleotide Archive (ENA) under BioProject accession **PRJEB110290**, https://www.ebi.ac.uk/ena/browser/view/PRJEB110290. All other datasets supporting

the conclusions of this article (DEG lists, enrichment, counts, qPCR, Sanger amplicon consensus sequences, per-library QC) are included within the article and its additional files. Analysis scripts, figure code, plant material and primers are available from the corresponding author on reasonable request, plant material subject to phytosanitary regulations.

Competing interests

The authors declare that they have no competing interests.

Funding

The author(s) declare that financial support was received for the research and/or publication of this article. This research was partly funded by the Federal Ministry of Food and Agriculture (BMEL), Germany under grant number 2818714A19, managed by the Federal Office for Agriculture and Food (BLE) and by grant P4-0077 from ARIS, Slovenia.

Authors' contributions

MH acquired funding, conceived and led the study, designed the qPCR assays and primers for quantitative validation, organised sequencing through a service provider, performed the bioinformatic analysis, prepared the figures and wrote the manuscript. SJ carried out CBCVd inoculation, plant management, sampling, RNA/sample extraction, library sequencing, and the Sanger and qPCR confirmation of the viroid infection, and contributed to the Methods and manuscript. UB performed the in vitro RNA synthesis of the inoculum and the quantitative RT-qPCR, and developed and adapted the qPCR protocol. JJ provided

bioinformatic input and strategic contributions to the manuscript. All authors read and approved the final manuscript.

Acknowledgements

The authors thank Joshua Faiß, Torsten Hüller and Elke Sprich for their support with sampling, measurements and plant care.

References

1. Jakše J, Radišek S, Pokorn T, Matoušek J, Javornik B. Deep-sequencing revealed citrus bark cracking viroid (CBCVd) as a highly aggressive pathogen on hop. Plant Pathol. 2015;64:831-42. https://doi.org/10.1111/ppa.12325

2. Julius Kühn-Institut. First finding of citrus bark cracking viroid (CBCVd) in Germany (Bavaria). 2019. https://pflanzengesundheit.julius-kuehn.de/dokumente/upload/CBCVd_pr2019-08by.pdf. Accessed 4 Sep 2026

3. Eiras M, de Oliveira AM, de Fátima Ramos A, Harakava R, Daròs JA. First report of citrus bark cracking viroid and hop latent viroid infecting hop in commercial yards in Brazil. J Plant Pathol. 2023;105:603. https://doi.org/10.1007/s42161-023-01313-4

4. Puchta H, Ramm K, Sänger HL. The molecular structure of hop latent viroid (HLV), a new viroid occurring worldwide in hops. Nucleic Acids Res. 1988;16:4197-216. https://doi.org/10.1093/nar/16.10.4197

5. Jagani S, Krönauer C, Born U, Hagemann MH. Viroid ecology in hops (*Humulus lupulus* L.): high prevalence in commercial systems but low presence in wild populations. Front Microbiol. 2026;16:1652923. https://doi.org/10.3389/fmicb.2025.1652923

6. Patzak J, Henychová A, Krofta K, Svoboda P, Malířová I. The influence of hop latent viroid (HLVd) infection on gene expression and secondary metabolite contents in hop (*Humulus lupulus* L.) glandular trichomes. Plants (Basel). 2021;10:2297. https://doi.org/10.3390/plants10112297

7. Hagemann MH, Treiber C, Born U, Schrader G, Stampfl J, Jakše J, et al. Risk potential of international fruit trade for viroid spreading - case study on hop viroids in Europe. J Plant Pathol. 2023;105:1335-46. https://doi.org/10.1007/s42161-023-01449-3

8. Sano T, Yoshida H, Goshono M, Monma T, Kawasaki H, Ishizaki K. Characterization of a new viroid strain from hops: evidence for viroid speciation by isolation in different host species. J Gen Plant Pathol. 2004;70:181-7. https://doi.org/10.1007/s10327-004-0105-z

9. Kappagantu M, Nelson ME, Bullock JM, Kenny ST, Eastwell KC. Hop stunt viroid: effects on vegetative growth and yield of hop cultivars, and its distribution in Central Washington State. Plant Dis. 2017;101:607-12. https://doi.org/10.1094/PDIS-06-16-0884-RE

10. Clark SM, Vaitheeswaran V, Ambrose SJ, Purves RW, Page JE. Transcriptome analysis of bitter acid biosynthesis and precursor pathways in hop (*Humulus lupulus*). BMC Plant Biol. 2013;13:12. https://doi.org/10.1186/1471-2229-13-12

11. Pokorn T, Radišek S, Javornik B, Štajner N, Jakše J. Development of hop transcriptome to support research into host-viroid interactions. PLoS One. 2017;12:e0184528. https://doi.org/10.1371/journal.pone.0184528

12. Dechorgnat J, Nguyen CT, Armengaud P, Jossier M, Diatloff E, Filleur S, et al. From the soil to the seeds: the long journey of nitrate in plants. J Exp Bot. 2011;62:1349-59. https://doi.org/10.1093/jxb/erq409

13. Lezhneva L, Kiba T, Feria-Bourrellier AB, Lafouge F, Boutet-Mercey S, Zoufan P, et al. The *Arabidopsis* nitrate transporter NRT2.5 plays a role in nitrate acquisition and remobilization in nitrogen-starved plants. Plant J. 2014;80:230-41. https://doi.org/10.1111/tpj.12626

14. Štajner N, Radišek S, Mishra AK, Nath VS, Matoušek J, Jakše J. Evaluation of disease severity and global transcriptome response induced by citrus bark cracking viroid, hop latent viroid, and their co-infection in hop (*Humulus lupulus* L.). Int J Mol Sci. 2019;20:3154. https://doi.org/10.3390/ijms20133154

15. Mishra AK, Kumar A, Mishra D, Nath VS, Jakše J, Kocábek T, et al. Genome-wide transcriptomic analysis reveals insights into the response to citrus bark cracking viroid (CBCVd) in hop (*Humulus lupulus* L.). Viruses. 2018;10:570. https://doi.org/10.3390/v10100570

16. Joubert M, van den Berg N, Theron J, Swart V. Transcriptomics advancement in the complex response of plants to viroid infection. Int J Mol Sci. 2022;23:7677. https://doi.org/10.3390/ijms23147677

17. Márquez-Molins J, Villalba-Bermell P, Corell-Sierra J, Pallás V, Gomez G. Integrative time-scale and multi-omics analysis of host responses to viroid infection. Plant Cell Environ. 2023;46:2909-27. https://doi.org/10.1111/pce.14647

18. Góra-Sochacka A, Więsyk A, Fogtman A, Lirski M, Zagórski-Ostoja W. Root transcriptomic analysis reveals global changes induced by systemic infection of *Solanum lycopersicum* with mild and severe variants of potato spindle tuber viroid. Viruses. 2019;11:992. https://doi.org/10.3390/v11110992

19. Mishra AK, Duraisamy GS, Matoušek J, Radišek S, Javornik B, Jakše J. Identification and characterization of microRNAs in *Humulus lupulus* using high-throughput sequencing and

their response to citrus bark cracking viroid (CBCVd) infection. BMC Genomics. 2016;17:919. https://doi.org/10.1186/s12864-016-3271-4

20. Guček T, Jakše J, Radišek S. Optimization and validation of singleplex and multiplex RT-qPCR for detection of citrus bark cracking viroid (CBCVd), hop latent viroid (HLVd), and hop stunt viroid (HSVd) in hops (*Humulus lupulus*). Plant Dis. 2023;107:3592–601. https://doi.org/10.1094/PDIS-11-22-2606-RE

21. Treiber C, Majer A, Born U, Kamp J, Schrader G, Stampfl J, et al, Possible import routes and sequence variations of the Citrus bark cracking viroid in German hops. In: Proceedings of the Scientific-Technical Commission, International Hop Growers' Convention, Lugo, Spain, 3–7 July 2022. p. 71–78. ISSN 1814-2206.

22. Martin M. Cutadapt removes adapter sequences from high-throughput sequencing reads. EMBnet J. 2011;17:10-2. https://doi.org/10.14806/ej.17.1.200

23. Dobin A, Davis CA, Schlesinger F, Drenkow J, Zaleski C, Jha S, et al. STAR: ultrafast universal RNA-seq aligner. Bioinformatics. 2013;29:15-21. https://doi.org/10.1093/bioinformatics/bts635

24. Padgitt-Cobb LK, Pitra NJ, Matthews PD, Henning JA, Hendrix DA. An improved assembly of the "Cascade" hop (*Humulus lupulus*) genome uncovers signatures of molecular evolution and refines time of divergence estimates for the Cannabaceae family. Hortic Res. 2023;10:uhac281. https://doi.org/10.1093/hr/uhac281

25. Danecek P, Bonfield JK, Liddle J, Marshall J, Ohan V, Pollard MO, et al. Twelve years of SAMtools and BCFtools. Gigascience. 2021;10:giab008. https://doi.org/10.1093/gigascience/giab008

26. Liao Y, Smyth GK, Shi W. featureCounts: an efficient general purpose program for assigning sequence reads to genomic features. Bioinformatics. 2014;30:923-30. https://doi.org/10.1093/bioinformatics/btt656

27. Robinson MD, McCarthy DJ, Smyth GK. edgeR: a Bioconductor package for differential expression analysis of digital gene expression data. Bioinformatics. 2010;26:139-40. https://doi.org/10.1093/bioinformatics/btp616

28. Pertea G, Pertea M. GFF utilities: GffRead and GffCompare. F1000Res. 2020;9:304. https://doi.org/10.12688/f1000research.23297.2

29. Buchfink B, Xie C, Huson DH. Fast and sensitive protein alignment using DIAMOND. Nat Methods. 2015;12:59-60. https://doi.org/10.1038/nmeth.3176

30. Alexa A, Rahnenführer J, Lengauer T. Improved scoring of functional groups from gene expression data by decorrelating GO graph structure. Bioinformatics. 2006;22:1600-7. https://doi.org/10.1093/bioinformatics/btl140

31. Subramanian A, Tamayo P, Mootha VK, Mukherjee S, Ebert BL, Gillette MA, et al. Gene set enrichment analysis: a knowledge-based approach for interpreting genome-wide expression profiles. Proc Natl Acad Sci U S A. 2005;102:15545-50. https://doi.org/10.1073/pnas.0506580102

32. Korotkevich G, Sukhov V, Budin N, Shpak B, Artyomov MN, Sergushichev A. Fast gene set enrichment analysis. bioRxiv. 2021. https://doi.org/10.1101/060012

33. Jagani S, Born U, Winterhagen P, Schrader G, Hagemann MH. Detection and persistence of citrus bark cracking viroid and other viroids in citrus peel oils for

agricultural applications. J Plant Pathol. 2025;107:1773-84. https://doi.org/10.1007/s42161-025-01953-8

34. Untergasser A, Cutcutache I, Koressaar T, Ye J, Faircloth BC, Remm M, et al. Primer3—new capabilities and interfaces. Nucleic Acids Res. 2012;40:e115. https://doi.org/10.1093/nar/gks596

35. Hagemann MH, Born U, Weber G, Wünsche JN. Gene structure and allelic variations of hop (*Humulus lupulus* L.) bitter acid biosynthesis genes. BrewingScience. 2019;72:207-16. https://doi.org/10.23763/BrSc19-25hagemann

36. Cock PJA, Antao T, Chang JT, Chapman BA, Cox CJ, Dalke A, et al. Biopython: freely available Python tools for computational molecular biology and bioinformatics. Bioinformatics. 2009;25:1422-3. https://doi.org/10.1093/bioinformatics/btp163

37. Kale SM, Gundlach H, Gericke O, Kamal N, Almeida A, Pitra N, et al. Extensive variation between chromosomes of North American and European hop. Nat Commun. 2026;17:4110. https://doi.org/10.1038/s41467-026-72379-8

38. Söderman E, Mattsson J, Engström P. The *Arabidopsis* homeobox gene ATHB-7 is induced by water deficit and by abscisic acid. Plant J. 1996;10:375-81. https://doi.org/10.1046/j.1365-313X.1996.10020375.x

39. Graether SP, Boddington KF. Disorder and function: a review of the dehydrin protein family. Front Plant Sci. 2014;5:576. https://doi.org/10.3389/fpls.2014.00576

40. Vashi J, Pathak A, Wany A, Kumar A. Role of nitrate transporters in plant defense. Physiol Mol Plant Pathol. 2025;140:102912. https://doi.org/10.1016/j.pmpp.2025.102912

41. Nacry P, Bouguyon E, Gojon A. Nitrogen acquisition by roots: physiological and developmental mechanisms ensuring plant adaptation to a fluctuating resource. Plant Soil. 2013;370:1-29. https://doi.org/10.1007/s11104-013-1645-9

42. Xia C, Li S, Hou W, Fan Z, Xiao H, Lu M, et al. Global transcriptomic changes induced by infection of cucumber (*Cucumis sativus* L.) with mild and severe variants of hop stunt viroid. Front Microbiol. 2017;8:2427. https://doi.org/10.3389/fmicb.2017.02427

43. Llave C. Dynamic cross-talk between host primary metabolism and viruses during infections in plants. Curr Opin Virol. 2016;19:50-5. https://doi.org/10.1016/j.coviro.2016.06.013

44. Więsyk A, Iwanicka-Nowicka R, Fogtman A, Zagórski-Ostoja W, Góra-Sochacka A. Time-course microarray analysis reveals differences between transcriptional changes in tomato leaves triggered by mild and severe variants of potato spindle tuber viroid. Viruses. 2018;10:257. https://doi.org/10.3390/v10050257

45. Martin K, Singh J, Hill JH, Whitham SA, Cannon SB. Dynamic transcriptome profiling of bean common mosaic virus (BCMV) infection in common bean (*Phaseolus vulgaris* L.). BMC Genomics. 2016;17:613. https://doi.org/10.1186/s12864-016-2976-8

46. Liu Y, Liu Y, Spetz C, Li L, Wang X. Comparative transcriptome analysis in *Triticum aestivum* infecting wheat dwarf virus reveals the effects of viral infection on phytohormone and photosynthesis metabolism pathways. Phytopathol Res. 2020;2:3. https://doi.org/10.1186/s42483-019-0042-6

47. Hou LY, Wu CH, Lin NS. Bamboo mosaic virus-induced metabolic reprogramming engages mitochondrial function to regulate redox homeostasis and defense responses in *Nicotiana benthamiana*. BMC Plant Biol. 2026;26:173. https://doi.org/10.1186/s12870-025-07996-4

48. Jeger MJ. Tolerance of plant virus disease: its genetic, physiological, and epidemiological significance. Food Energy Secur. 2023;12:e440. https://doi.org/10.1002/fes3.440

49. Bengyella L, Waikhom SD, Allie F, Rey C. Virus tolerance and recovery from viral induced-symptoms in plants are associated with transcriptome reprograming. Plant Mol Biol. 2015;89:243-52. https://doi.org/10.1007/s11103-015-0362-6

50. Sečnik A, Volk H, Kunej U, Radišek S, Štajner N, Jakše J. Genome-wide DNA methylation analysis of CBCVd-infected hop plants (*Humulus lupulus* var. "Celeia") provides novel insights into viroid pathogenesis. Microbiol Spectr. 2025;13:e00394-24. https://doi.org/10.1128/spectrum.00394-24

51. Pesti R, Kontra L, Paul K, Vass I, Csorba T, Havelda Z, et al. Differential gene expression and physiological changes during acute or persistent plant virus interactions may contribute to viral symptom differences. PLoS One. 2019;14:e0216618. https://doi.org/10.1371/journal.pone.0216618

52. Paudel DB, Montenegro Alonso AP, Chisholm J, Xiao H, Sanfaçon H. Transcriptomic changes associated with infection of *Nicotiana benthamiana* plants with tomato ringspot virus (genus *Nepovirus*) during the acute symptomatic stage and after symptom recovery. PLoS One. 2025;20:e0328517. https://doi.org/10.1371/journal.pone.0328517

Additional files

Additional file 1. *File format:* .pdf. *Title of data:* Supplementary Information (Supplementary Notes 1–6 and Supplementary Figures S1–S13). *Description of data:* Six thematic Supplementary Notes, each with its figures, in order of citation in the main text: Note 1, leaf proline (assay, Fig. S1); Note 2, sequencing and mapping quality control (Figs. S2 and S12); Note 3, differential-expression overview and sensitivity analyses with

alternative models (Figs. S3–S4); Note 4, GO and KEGG gene-set enrichment (Figs. S5–S8); Note 5, qPCR validation, Sanger amplicon confirmation and NRT2 family phylogeny (Figs. S9 and S13); Note 6, reference-genome comparison of Cascade, Kew and Apollo (Figs. S10–S11).

Additional file 2. *File format:* .xlsx. *Title of data:* Supplementary Tables ST1–ST20. *Description of data:* Processed datasets in one workbook, one worksheet per table, with a contents sheet, including the Sanger consensus sequences (ST11) and the raw and TMM-normalised count matrices (ST15a, ST15b). Worksheets: ST1 leaf proline data; ST2 per-library sequencing/mapping QC; ST3 DEGs May (162); ST4 DEGs August (12); ST5 persistent DEGs (1, May ∩ August); ST6 genes with significant treatment × timepoint interaction (12); ST7 GSEA GO/KEGG (May/August/interaction); ST8 ORA per timepoint (GO/KEGG); ST9 qPCR primers (forward/reverse sequence, length, GC %; designed in this study) and the HLVd detection probe; ST10 qPCR × RNA-seq correlation; ST11 Sanger amplicon consensus sequences; ST12 Cascade↔Kew reciprocal best hits (genome-wide); ST13 Kew cross-validation of the Cascade DEGs; ST14 hop NRT2 gene family; ST15 raw (a) and TMM-normalised (b) count matrices; ST16 leave-one-library-out sensitivity analysis; ST17 virus and viroid reads per library; ST18 HLVd and CBCVd RT-qPCR of the experimental plants (September 2022); ST19 mixed-model results for chlorophyll, proline and biomass; ST20 blastn re-annotation of the DEGs without a SwissProt hit.

Supplementary Files

This is a list of supplementary files associated with this preprint. Click to download.

- Additionalfile1SupplementaryInformation.docx
- Additionalfile2SupplementaryTables.xlsx